Improved Power Quality in a Solar PV Plant Integrated Utility Grid by Employing a Novel Adaptive Current Regulator

V. Narendra Kumar, Narendra Babu P, R. Kiranmayi, Pierluigi Siano, *Senior Member, IEEE*, and Gayadhar Panda, *Senior Member, IEEE*

***Abstract*—Integration of solar photovoltaic plants into the distribution systems using various power processing units produces the harmonics that may cause malfunctioning of sensitive equipment connected to the point of common coupling. To overcome this drawback, a novel adaptive current regulator is employed for the grid interfacing voltage source inverter. In addition, a high-gain dc–dc converter with a Kalman-based maximum power point tracking algorithm is designed to achieve the high voltage level at the common dc bus. To determine three-phase reference currents, the proposed adaptive current regulator is designed by using a recurrent neural network trained with the Hebbian least mean square weight updating algorithm. They are used to generate the three-phase compensating currents for suppressing the harmonics present in the system. The proposed method has several merits, such as better harmonic mitigation ability, adaptive behavior, improved stability, and lesser settling time, as compared with the conventional PI controller. The system performance with the proposed current control regulator is analyzed via MATLAB/Simulink. Comparative analysis via simulation platform assures the improved performance in terms of power quality, settling time, and stability of the proposed controller. Also, the effectiveness of the proposed controller is validated under several transient conditions by developing a laboratory scale prototype model with the dSPACE control desk.**

***Index Terms*—Hebbian least mean square (LMS), high-gain converter, Kalman-based maximum power point tracking (MPPT), power quality, proportional–integral, photovoltaic (PV) system, recurrent neural network (RNN).**

Nomenclature

P_{pv}	Instantaneous power generated by a photovoltaic source (W).
L_1	Primary inductance of the coupled inductor (H).
L_2	Secondary inductance of the coupled inductor (H).
L_k	Leakage inductance of the coupled inductor (H).
L_m	Magnetizing inductance of the coupled inductor (H).
C_1	Capacitance of the passive clamp circuit (F).
n	Turns ratio of the coupled inductor.
d	Duty ratio supplied to a MOSFET switch of the converter.
V_{error}	DC-link voltage deviation (V).
$I_{\text{ref}}(s)$	Reference current generated from controller.

Manuscript received June 14, 2019; revised August 20, 2019, September 11, 2019, and December 6, 2019; accepted December 6, 2019. This work was supported in part by the RECTPCL-CSR Funded Project under Grant RECTPCL/CSR/2016-17/693. *(Corresponding author: Narendra Babu P.)*

V. N. Kumar and R. Kiranmayi are with the Electrical Engineering Department, Jawaharlal Nehru Technological University Anantapur, Anantapur 515002, India (e-mail: narendrakumar.abc@gmail.com; kiranmayi0109@gmail.com).

N. B. P and G. Panda are with the Electrical Engineering Department, National Institute of Technology Meghalaya, Shillong 793003, India (e-mail: narem.perumal@nitm.ac.in; gayadhar.panda@nitm.ac.in).

P. Siano is with the Department of Management and Innovation Systems, University of Salerno, 84084 Fisciano, Italy (e-mail: psiano@unisa.it).

Digital Object Identifier 10.1109/JSYST.2019.2958819

I. Introduction

RENEWABLE power injection to existing utility grid is becoming essential to meet the electricity demand in the future to come. The massive penetration of renewable energy sources (RES) can reduce the use of fossil-fuel as well as protect the environment from greenhouse gas emission. These factors are the driving force for the researchers to orient their research work toward integration of RES to the utility grid along with their operation and control [1].

Among existing renewable sources, photovoltaic (PV) based power generation has the better performance characteristics [2]. However, it has few limitations like low generating voltages, difficult in tracking maximum power point (MPP) due to sporadic nature of solar irradiance, and poor power quality due to the presence of power electronic converters and varying connected loads in the system [3]–[5]. DC–DC boost converters are utilized to match low voltages of the PV system at the common dc-link bus terminals. The drawbacks with the conventional dc–dc converters are sudden rise in input current, high power loss during switching, and maximum diode reverse current [6]. Hence, dc microgrid associated with the conventional converters suffers from more losses, high strain, and less efficiency [7], [8]. In [34], Ghiasi has provided the technical and economic evaluation of renewable energy systems with power quality utilized by the FACTS devices. Moreover, an optimization-based power quality change method has been given for delivering differentiated power quality in grid-tied renewable energy systems. In [35] and [36], Liu *et al.* have proposed a transformer-based filtering topology for power quality enrichment and management in the dc source system of industrial application and the PV power plant. Moreover, the effect of the weak coupling of integrated reactor on the filtering performance and the residual weak coupling, and the electromagnetic decoupling model of transformer-based filtering topology have been analyzed.

In order to defeat the difficulties incorporated with conventional converters, a high-gain, high-efficient power processing units are employed for the microgrid system. In this article, a novel scheme of high-gain more-efficient power processing unit using coupled inductor connected in the interleaved manner [9],

passive clamp circuit, and a storage capacitor along with Kalman MPPT is presented. This high-gain converter improves the low voltage level of the PV system even with less duty ratio and reduced loss.

Integration of RES to the utility grid is very much essential for the present power scenario to reduce greenhouse gas effect [10]. Hence, the PV power conversion requires better power quality by regulating the voltage and frequency deviations. Therefore, an accurate and faster controller is required for the operation of grid-connected converters. Also, a filter circuit is required for removing the harmonics generated by the power electronic components [11], [12]. However, the inclusion of filter circuit causes instability problem. This results difficulty for controlling the voltage source inverter (VSI) [13]. The existing current controller produces unstable and damping controller action while controlling the grid connected VSI [14].

Control of grid-connected systems has moved away from the conventional single-loop control to performance-oriented dual loop control, i.e., voltage- and current-control loops. Maintaining the quality of power being injected into the grid, the current control loop plays a vital role in the grid connected system [15]. It is devised in the literature [16] that a PI current controller is employed for grid-connected inverters to establish the output current to follow a certain reference current, which is obtained from required power transfer to utility grid. Prime limitation of the PI current controller is its inability to operate effectively under unbalanced conditions. The PI current controller generally fails to follow a sinusoidal reference without the steady-state error. Therefore, a nonlinear intelligent technique with recurrent neural network (RNN) has been employed to reduce the harmonics produced in the system, and also to get superior control over grid injected reactive power [17]. RNN is an effective control technique compared with the conventional control schemes because of its self-adjustment capability during system parameter variations, and it works well under the noisy conditions. It also provides better performance during large load change [18]. The performance of the proposed RNN current controller mainly depends on the use of efficient training algorithm.

In this article, a novel adaptive [Hebbian least mean square (LMS) based RNN] current regulator is proposed to enhance the performance of a grid-connected VSI under various operating scenarios. The training of neurons present in the RNN current controller is performed using the Hebbian-LMS algorithm. It is a new unsupervised learning algorithm employed for RNN network to adapt automatically based on the varying operating scenarios [19]–[25]. This article addresses the main system components, control strategy, stability analysis, and experimental validation. The main novel research contributions of the proposed work are as follows.

1) An adaptive RNN trained with the Hebbian-LMS weight updating algorithm is employed to calculate the three-phase reference currents, which are used to generate the desired pulsewidth modulation signals for the grid interfacing inverter; in turn, it improves the power quality of the PV system.
2) A new high-gain dc–dc boost converter with a Kalman-based MPP tracking (MPPT) algorithm is designed to achieve the required voltage level at the dc-link bus terminals.
3) A comparative study of the proposed current regulator is performed with a conventional PI controller to demonstrate the effectiveness of the proposed technique under several transient conditions.
4) A study on the control stability of the proposed current regulator via both simulation and experimental platforms under several transient conditions is carried out, which demonstrates the better performance of the proposed scheme in terms of stability for a grid-connected PV system.

II. System Description

The qualitative power generated and transmitted through the grid integrated solar PV plant with a proposed novel control scheme is depicted in Fig. 1. The design building blocks of this control scheme are particularized as follows. The modeling as well as design specifications of the solar PV array is referred from the work in [26]. While designing the proposed system, a high-gain high-efficient dc–dc converter is being proposed to couple the solar plant with common dc bus. This type of converter not only enhances the efficiency but also increases the voltage level while reducing its stress and switching losses compared with existing topologies. Again, the Kalman MPPT control technique has been chosen to control the high-gain more-efficient converter with better performance [27]. Similarly, grid-side converter (i.e., VSI) is being controlled by using a dual-loop power flow technique. The power flow control technique usually comprises of an outer voltage control loop used to maintain a constant voltage level at the input of the VSI and an inner current control loop to establish improved power quality of grid currents. In this study, a novel inner loop control technique using the Hebbian-LMS trained RNN controller is also proposed. Moreover, VSI is connected to the utility grid through *LC* filters and step-up transformer.

III. Proposed Control Strategy

A. Kalman MPPT Algorithm

The switching pulses required for high-gain high-efficient dc–dc converter is produced by utilizing the Kalman MPPT control technique. For implementation of Kalman MPPT, the system is modeled with state-space equations. The state-space representation of a system is denoted as follows [27]:

$$x(k+1) = Ax(k) + Bu(k) + Gw(k) \tag{1}$$

$$z(k) = Cx(k) + V(k) \tag{2}$$

where $x(k)$ is the state, $u(k)$ is the input, $z(k)$ is the output signals, $w(k)$ corresponds to process noise and $v(k)$ represents measurement noise. Time update and measurement correction are done to estimate the actual voltage, given as follows:

Measurement update (correct)

$$K_{[k]} = H_{[k]^-} - [H_{[k]^-} + R]^{-1} \tag{3}$$

$$\hat{V}_{\mathrm{act}[k]} = \hat{V}_{\mathrm{act}[k]^-} + K_{[k]}[V_{\mathrm{ref}[k]} - \hat{V}_{\mathrm{act}[k]^-}] \tag{4}$$

$$H_{[k]} = [1 - K_{[k]}]H_{[k]^-}. \tag{5}$$

Time update (predict)

$$\hat{V}_{\mathrm{act}[k+1]} = \hat{V}_{\mathrm{act}[k]} + M\frac{P_{[k]} - P_{[k-1]}}{V_{[k]} - V_{[k-1]}} \tag{6}$$

$$H_{[k+1]^-} = H_{[k]} + Q. \tag{7}$$

Initially, the Kalman gain $K_{[k]}$ has to be calculated from (3). In the next step, calculated actual voltage $\hat{V}_{\mathrm{act}[k]}$ and error

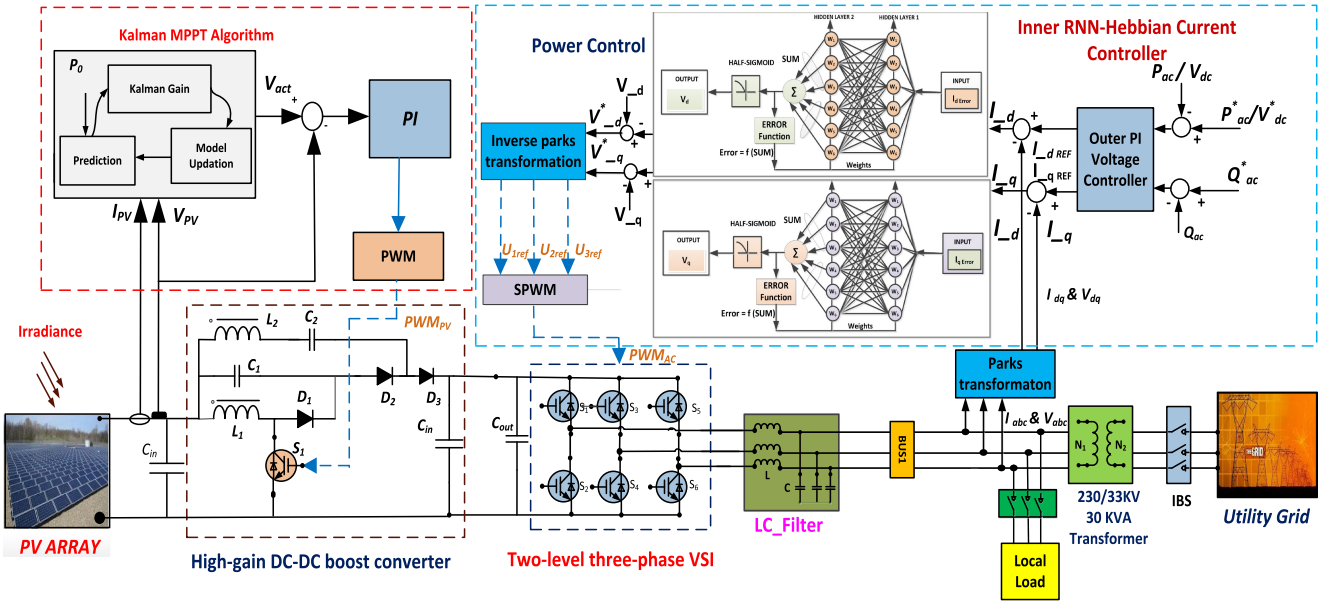

Fig. 1. Grid-connected PV system with a novel adaptive current regulator.

covariance H_k are to be updated correspondingly from (4) and (5). In time updating, the voltage $\hat{V}_{\text{act}[k+1]}$ and error covariance $H_{[k+1]^-}$ are to be predicted from $\hat{V}_{\text{act}[k]}$ and H_k, from (6) and (7). Finally, the estimated voltage $\hat{V}_{\text{act}[k+1]}$ will reach the MPP than $\hat{V}_{\text{act}[k]}$. Therefore, it can be established that the expected voltage $\hat{V}_{\text{act}[k+1]}$ is nearer to MPP than the real value $\hat{V}_{\text{act}[k]}$, where Q is the process noise of the plant, R is the measurement noise co-variance, and M is the step size.

The terminal voltage and currents are fed to the Kalman algorithm, it predicts the voltage in the next step. The voltage error between present voltage and estimated voltage is given to the PI controller to generate pulses for the dc–dc converter switch, as shown in Fig. 1.

B. Control of Voltage Source Inverter

The grid interfacing inverter (i.e., VSI) has to be controlled by means of a dual-loop power flow control technique. The power flow control technique is composed of outer-loop voltage and inner-loop current controllers. The voltage controller used in this article is a PI controller and the gains of this controller are chosen by the trial-and-error method. The conventional PI controller is used as an outer control loop, and the Hebbian-LMS trained RNN controller is used as the inner-loop current controller. RNN topology has good performance over the conventional neural network as it feeds back the output signals to the inputs for more precision, as shown in Fig. 1. The quicker response characteristic of the RNN-current control structure trained by the Hebbian-LMS algorithm helps in achieving system stability quickly and consequently following better power quality [28]. In turn, it has more stability and dynamic behavior over the feedforward network. Therefore, it is best suited for the closed-loop control applications [29], [30]. Thus, the deployment of proposed RNN inner current-loop control function maintains improved quality of currents to the utility grid. The active and reactive powers are regulated by d- and q-axis control loops.

The proposed RNN control scheme comprises two input terminals, two output terminals, and two hidden layers. The input signal of the RNN network is current errors, i.e., $I_{d,\text{error}}$ and $I_{q,\text{error}}$, which are expressed as follows:

$$\hat{I}_{d,\text{error}} = \hat{I}_d - \hat{I}_{d,\text{ref}} \tag{8}$$

$$\hat{I}_{q,\text{error}} = \hat{I}_q - \hat{I}_{q,\text{ref}}. \tag{9}$$

RNN current controller contains six weights consisting of two separate hidden layers. Six neurons are sufficient enough to obtain desired responses. By using two hidden layers, strong minimization of the error can be achieved. In this RNN current control, output of the structure is feedback to the input for getting more accurate result. This controller requires only current errors as inputs that make the architecture of the controller more easy and efficient. The initial weights of the neurons are calculated by the trial-and-error method. The output layer produces $d-q$ voltage control signals in order to generate the pulses for the grid-side converter (VSI). The RNN current controller can be represented as R $(\hat{I}_{dq}(k), \hat{V}_{dq}(k), \hat{W})$, which is a function of $\hat{V}_{dq}$, $\hat{I}_{dq}$ and network weights $\hat{W}_.$, and $\hat{W}^-$ denotes all the weights correspond at each hidden layer. More evidently, R $(\hat{I}_{dq}(k), \hat{V}_{dq}(k), \hat{W})$ is given as

$$R(\hat{I}_{dq}(k), \hat{V}_{dq}(k), \hat{W}) = (\hat{W}_2(\hat{W}_1 \times \hat{V}_{dq}(k))) \tag{10}$$

where $\hat{W}_1$ represents the weights of the first hidden layer, and $\hat{W}_2$ represents the weights of the second hidden layer.

After the weights are finalized, it is to be updated at each iteration corresponding to the error for reaching the desired response. The updating or training of RNN is done with the help of the Hebbian-LMS algorithm to achieve the better performance compared with the available algorithms. It is supplied to the neurons to get the required error signal.

The error signal obtained is the sum of all weights at each hidden layer. The structure of the Hebbian-LMS algorithm is

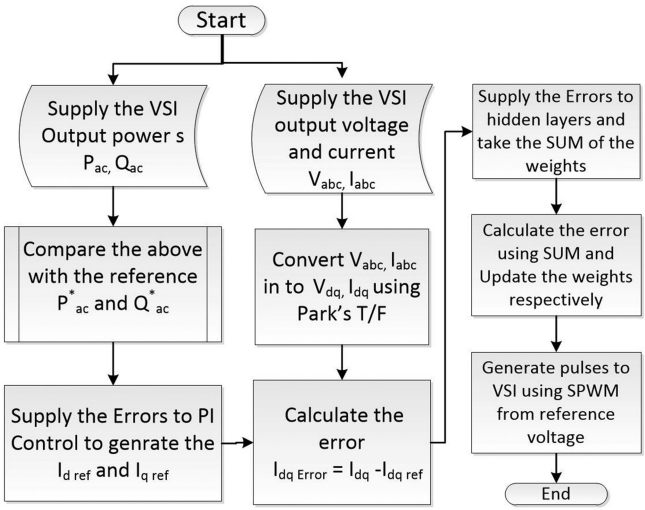

Fig. 2. Power flow control for producing pulses to VSI.

TABLE I
SYSTEM PARAMETERS

Parameter	Value
Grid frequency (f_p)	50Hz
Nominal Power (P)	30 kW
PV array voltage (V_{pv})	300 V
PV array current (I_{pv})	100 A
Grid Inverter Voltage (L-L)	500 V
Grid Inverter Current (L-L)	40 A
Grid Side Transformer (δ / Y)	30 KVA, 230V/33KV
Grid Side Capacitor (C_f)	22 pF
Grid Side Inductor (L_f)	150 mH
Grid Side Local Load (R-L)	20 KW (Maximum)

TABLE II
CONTROL PARAMETERS USED FOR ANALYSIS

Parameter	Value
$V_{DC,Ref}$	500 V
RNN (K_p ,K_i)	0.7,80
Weights of Neurons (W_1 to W_6)	0.028
Switching frequency	20 KHz
Sampling period	5 μs
Kalman filter (Q and R)	0.04, 0.008

shown in Fig. 1. The learning algorithm can be expressed as

$$w_{k+1} = w_k + 2\mu e_k X_k \tag{11}$$

$$e_k = f((\text{sum})_k) = f(X_k^T, w_k). \tag{12}$$

The neuron output can be given as

$$\text{Out}_k = \begin{cases} \text{SGM}((\text{sum})_k) = \text{SGM}(X_k^T, w_k), & \text{for}(\text{sum})_k > 0 \\ \text{other wise} \quad 0, & \text{for}(\text{sum})_k < 0. \end{cases} \tag{13}$$

In this way, the error is minimized quickly and accurately by using an RNN current controller. The total power flow control chart for controlling the VSI is shown in Fig. 2.

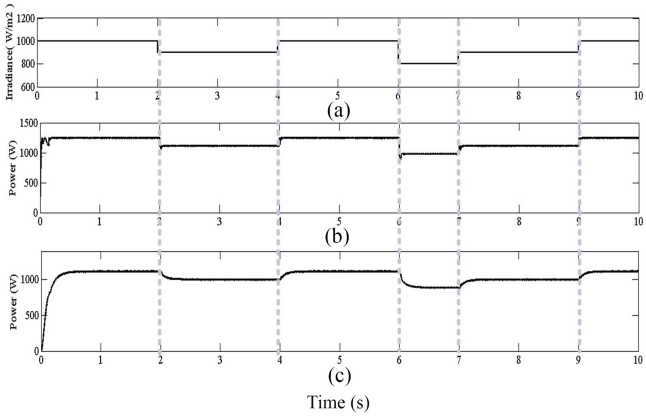

Fig. 3. (a) Step change in irradiance (W/m^2). (b) Kalman MPPT output power (W). (c) INC MPPT output power (W).

IV. STABILITY ANALYSIS

A. System Stability

The system considered is of nonlinear nature due to its power electronic devices, temperature variations, parameter changes in passive components, ageing effects, etc. Lyapunov stability theorem is employed to find out the dynamics of these type of systems [17], [31]. It is the best technique used for analyzing stability, asymptotic stability, and exponential stability. The direct method of a Lyapunov stability criterion for stability is given as follows.

1) An energy function represented as $V_{(x)}$ is to be selected such that $V_{(0)} = 0$ and $V_{(x)} \geq 0 \; \forall \; x \in D$, where x is a state variable, and D is the real domain.
2) $\hat{V}(x)0 \quad \forall \; x \in$ D; therefore, it can be assured that $V(x)$ decreases corresponding to the time and the chosen system is stable.

The dc-link voltage (V_{dc}) gives the information about excess or deficit power available at common bus-bar. The power balance equation can be given as

$$P_{\text{pv}} = P_{\text{dc}} + P_{\text{ac}}. \tag{14}$$

It can also be written as

$$I_{\text{pv}} \times V_{\text{pv}} = I_{\text{dc}} \times V_{\text{dc}} + \frac{3}{2}(i_{gd} \times v_{gd} + i_{gq} \times v_{gq}). \tag{15}$$

The previous expression can also be written in the following manner:

$$I_{\text{pv}} = I_{\text{dc}} + \frac{3}{2}(i_{gd} + i_{gq}). \tag{16}$$

The disturbance occurs in the previous equation, it becomes

$$\triangle I_{\text{pv}} = \triangle I_{\text{dc}} + \frac{3}{2}(\triangle i_{gd} + \triangle i_{gq}). \tag{17}$$

Rearranging the previous equation

$$C_{\text{dc}} \triangle V_{\text{dc}} = \triangle I_{\text{pv}} - \frac{3}{2}(\triangle i_{gd} + \triangle i_{gq}). \tag{18}$$

The Lyapunov energy function can be selected as

$$V = \frac{1}{2}(C_{\text{dc}} \triangle V_{\text{dc}}^2). \tag{19}$$

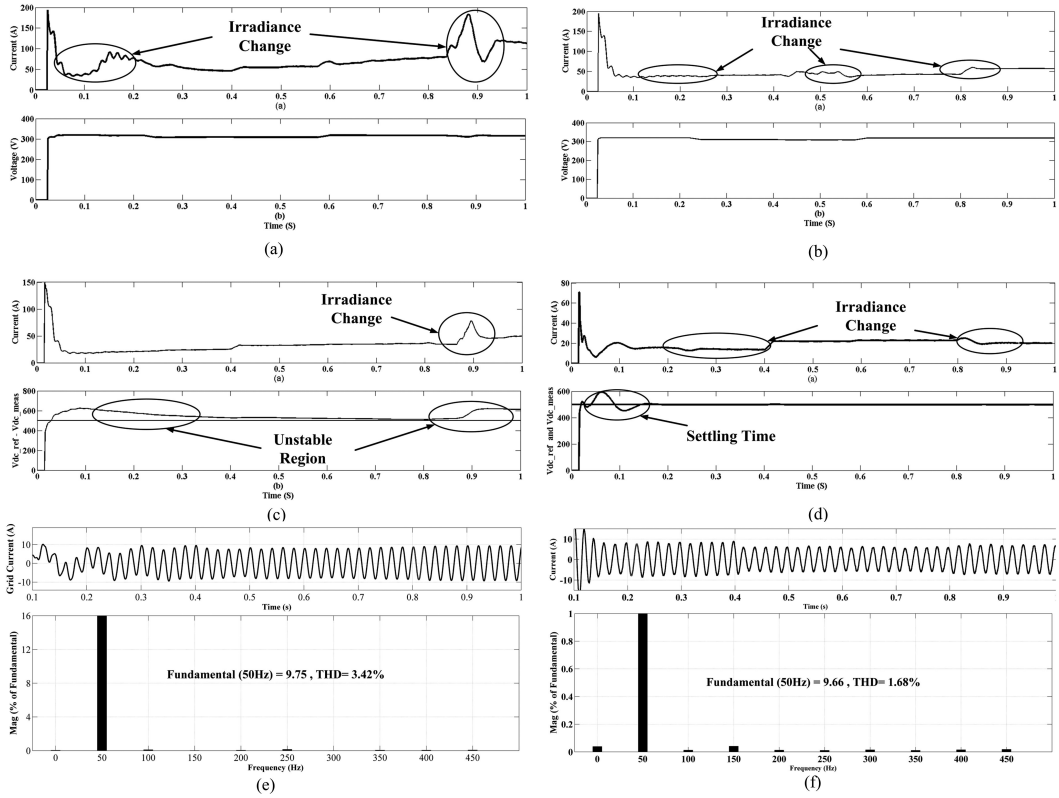

Fig. 4. Performance parameters. Case 1: (a) and (b) Point of common coupling (PCC) terminal current and voltage. (c) and (d) Current and voltage at common dc bus. (e) and (f) %THD of grid-side current.

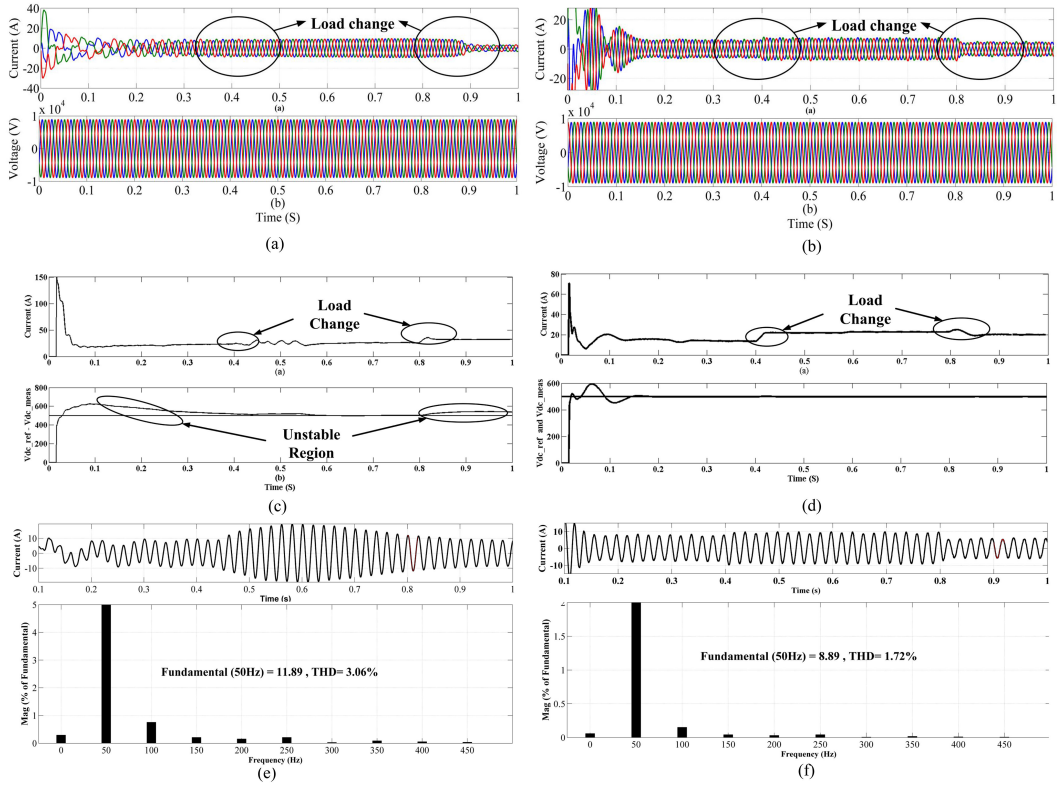

Fig. 5. Performance parameters. Case 2: (a) and (b) PCC terminal current and voltage. (c) and (d) Current and voltage at common dc bus. (e) and (f) %THD of grid-side current.

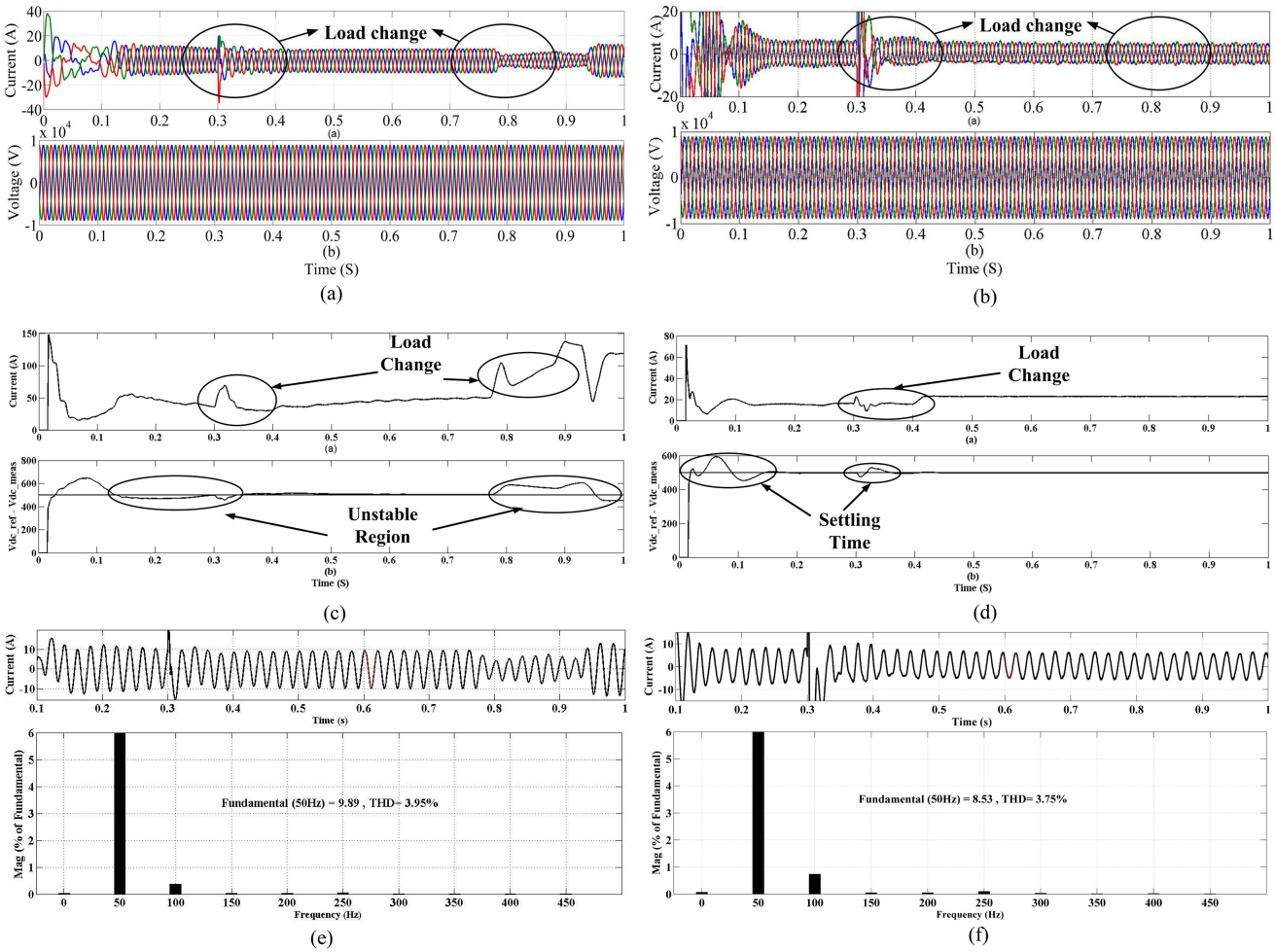

Fig. 6. Performance parameters. Case 3: (a) and (b) Grid-side current and voltage. (b) and (c) Current and voltage at common dc bus. (e) and (f) %THD of grid-side current.

Differentiating the previous equation

$$\dot{V} = (C_{\rm dc} \triangle V_{\rm dc} \triangle \dot{V}_{\rm dc}) \tag{20}$$

where $\triangle V_{\rm dc} = \triangle V_{\rm dc,ref} - V_{\rm dc}$

$$\dot{V} = (\triangle V_{\rm dc,ref} - V_{\rm dc}) \left[(\triangle I_{\rm pv}) - \frac{3}{2} (\triangle i_{gd} + \triangle i_{gq}) \right]. \tag{21}$$

The system proposed is grid connected; the excess PV power available at the common bus is transferred to the utility grid. If PV power is less than the load demand, it is compensated by the utility grid. The utility grid is assumed as a large reservoir of power, and hence, for small perturbation, the equation results negative or zero ($\triangle I_{\rm pv} \leq \triangle i_{gd}$, $\triangle i_{gq} \approx 0$, and $V_{\rm dc} \leq V_{\rm dc,ref}$). Therefore, $\dot{V}$ is negative semi-definite and the system is stable. If the system demands large power, then it should be isolated from the grid by monitoring continuously.

B. Control Stability

The proposed current controller stability is very important to show the improved performance of the system [32], [33]. The necessary conditions for the controller to be stable are given as follows. Assume that the expectation of the weight error vector is taken as

$$V_k \cong E(W^0 - W_k) \tag{22}$$

where W^0 is unknown system weights and W_k is RNN weights. The transformed V_k by Q is given as

$$\acute{V}_k \cong Q^T \times V_k. \tag{23}$$

The Eigen vector matrix is given as

$$R = Q \times A \times Q^T \tag{24}$$

where Q is the unitary matrix, and A is diagonal eigenvalue matrix. From the weight updating (11), the expectation is given as

$$E(W_{k+1}) = E(W_k) + 2 \times \mu E(e_k X_k) \tag{25}$$

$$E(W_{k+1}) = E(W_k) - 2 \times \mu \left[E(x_k x_k^T W_k) - E(d_k x_k) \right] \tag{26}$$

where d_k is the desired response, with the help of independent assumption, the previous equation becomes

$$E(W_{k+1}) = E(W_k) - 2 \times \mu [RE(W_k) - p]. \tag{27}$$

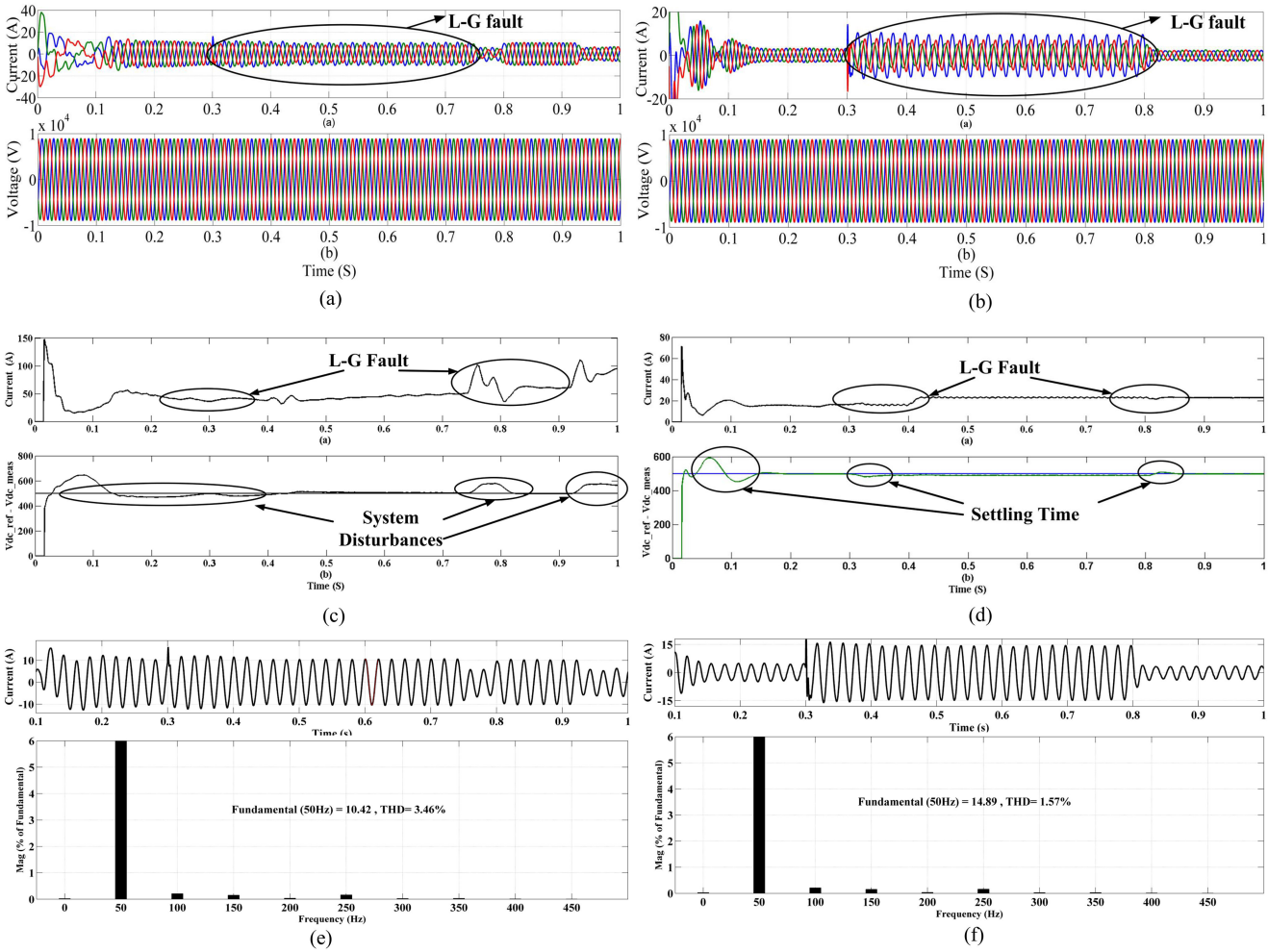

Fig. 7. Performance parameters. Case 4: (a) and (b) Grid-side current and voltage. (b) and (c) Current and voltage at common dc bus. (e) and (f) %THD of grid-side current.

From (25) and (26)

$$\acute{V}_k \cong (I - 2 \times \mu A)^n \times \acute{V}_0 \tag{28}$$

where $\acute{V}_0$ is the initial value, for each eigenvalue of λ_i of R, the respective mode is given as

$$\acute{v}_k(l) \cong (I - 2 \times \mu\lambda_i)^n \times \acute{v}_k(0). \tag{29}$$

Hence, there will be many modes for the different eigenvalues of R. As the step-size parameter μ fulfills the condition $0 \leq \mu \leq \frac{1}{\lambda'_{\max}}$, and then all the elements $\acute{v}_k(l)$ tend to be zero. Thus, the controller tends to convergence. The sufficient condition for the controller to be bound as $0 \leq \mu \leq \frac{1}{3Tr(R)}$. In this way, the controller stability can be analyzed.

V. Simulation Study

The solar PV array integrated with utility grid, shown in Fig. 1, is modeled and simulated via MATLAB 2014a /Simulink under different test cases. The system specifications and control parameters are presented in Tables I and II.

The Kalman MPPT power output is compared with the conventional incremental conductance MPPT algorithm (INC) to confirm its improved performance of settling time and output. Fig. 3 shows the power output from dc–dc converter of PV array with different irradiance levels. It is observed from Fig. 3 that Kalman MPPT shows improved output and settling time than the conventional INC MPPT control.

To assure the controller performance under different system conditions, it is analyzed under five different cases such as by changing solar irradiance, transient linear load, transient nonlinear load, L–G fault on grid side, and unbalanced grid voltage. These test cases are described as follows.

Test Case 1: In this study, Solar irradiance is changed with a step change from 1000 to 600 W/m^2 at $t = 0.2$ s and again it increased linearly in the duration of 0.6–0.8 s. In this case, the outer voltage loop is PI voltage regulator, and the inner current loops are PI and RNN controllers. Fig. 4(a), (c), and (e) shows the performance characteristics of the proposed system with conventional PI current controller, whereas Fig. 4(b), (d), and (f) shows the performance characteristics of the proposed system by employing Hebbian-LMS-RNN current controller. Fig. 4(a) and (b) shows the PV terminal voltage and current at the input of boost converter, and change in PV current corresponds to the irradiance change, respectively. Fig. 4(c) and (d) depicts corresponding the current and voltage characteristics of the

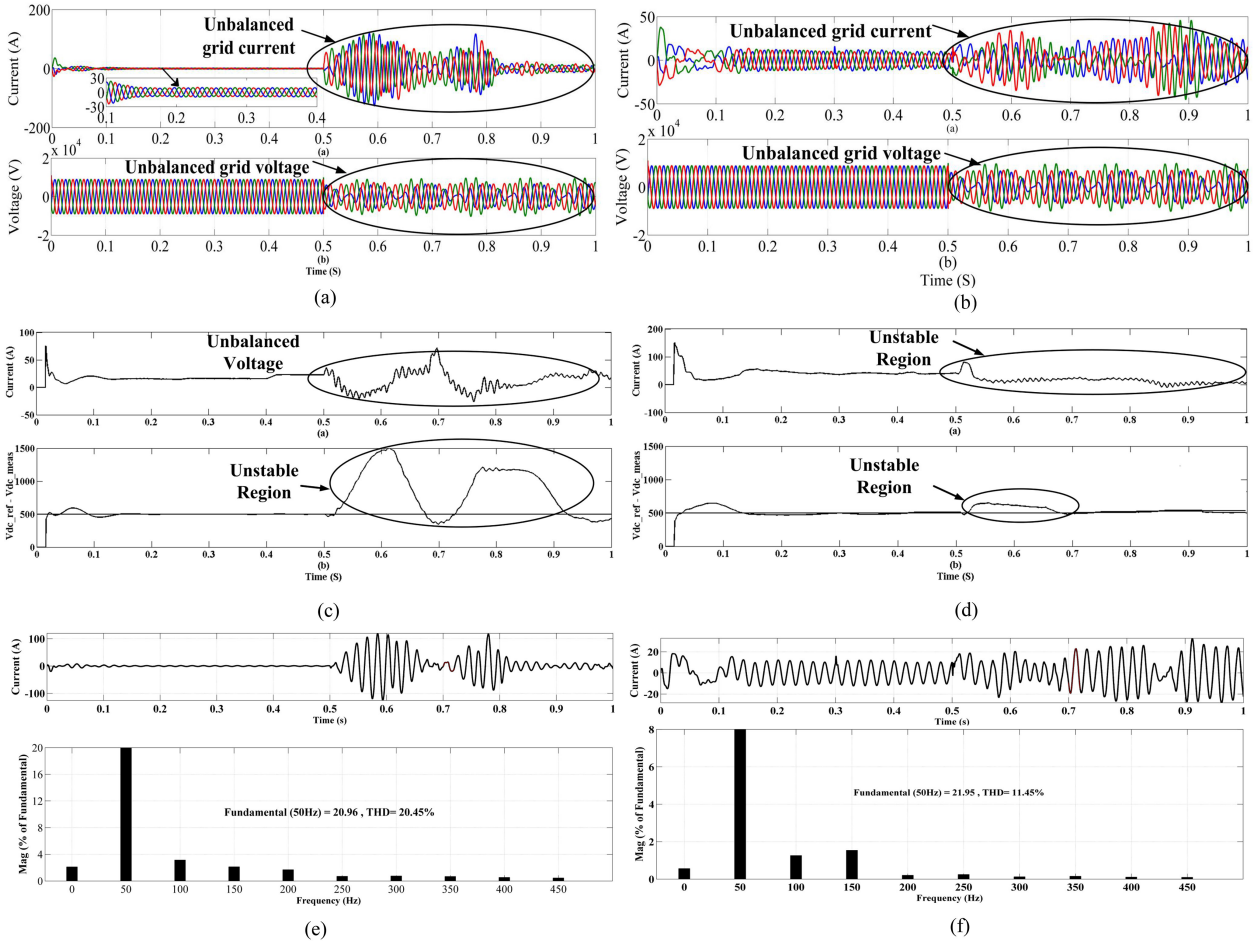

Fig. 8. Performance parameters. Case 5: (a) and (b) Grid-side current and voltage. (b) and (c) Current and voltage at common dc bus. (e) and (f) %THD of grid-side current.

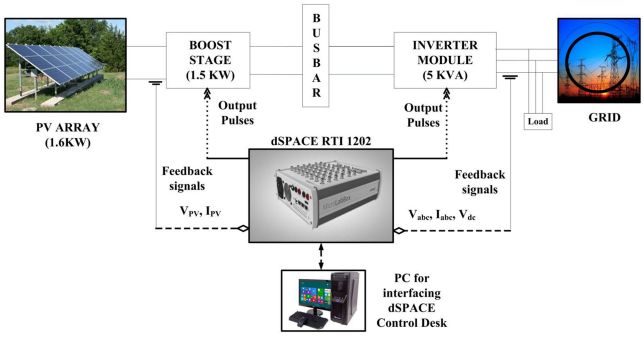

Fig. 9. Schematic structure of the hardware setup.

conventional PI controller and proposed RNN current controller at the common dc-link bus. By observing Fig. 4(c) and (d), the proposed RNN controller shows better stability performance over the conventional PI controller. Similarly, Fig. 4(e) and (f) shows %THD content for the grid current during solar irradiance change with PI and proposed RNN controller is 3.42% and 1.68%, respectively. THD content of the proposed controller has been found very less compared with the conventional controller.

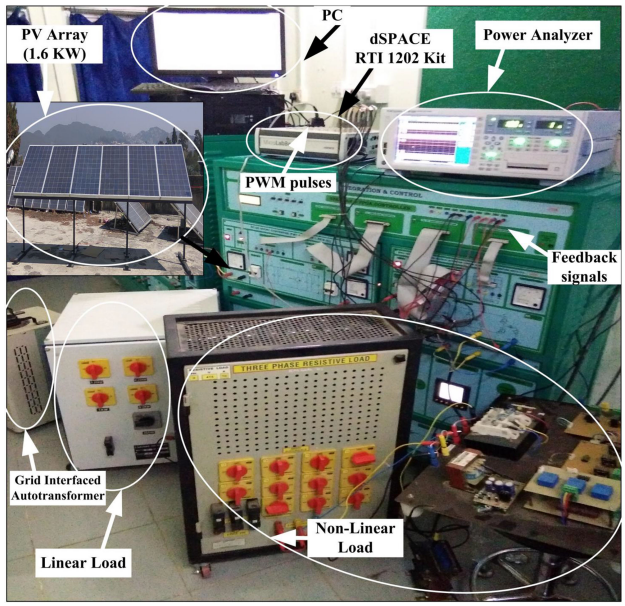

Fig. 10. Laboratory-level setup for the real-time analysis of the RNN controller.

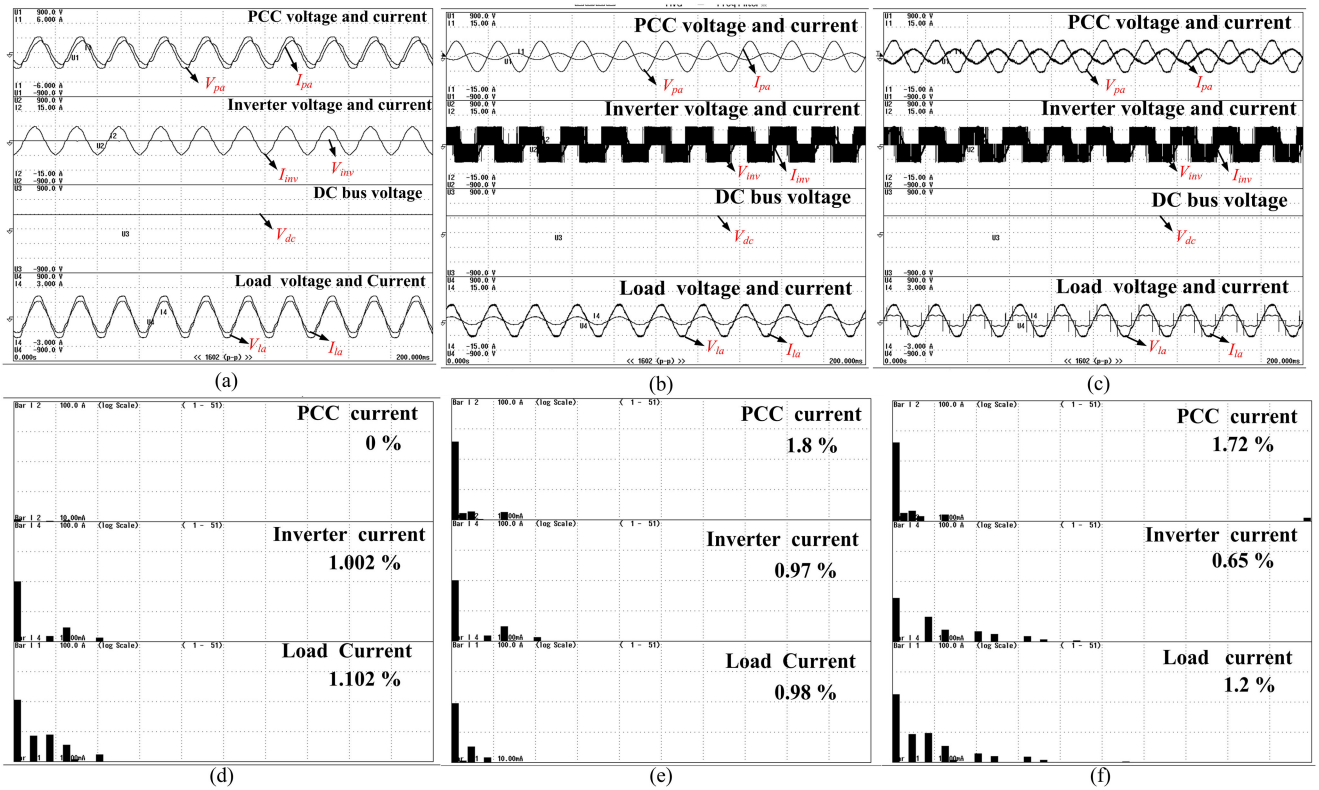

Fig. 11. Performance parameters: (a) Without $\mathrm{PV}_{\mathrm{linear\ load}}$. (b) With $\mathrm{PV}_{\mathrm{linear\ load}}$. (c) With $\mathrm{PV}_{\mathrm{nonlinear\ load}}$ (Scales: Time: 0.1 s/div., Voltage: 150 V/div., Current: 1 A/div.). %THD: (d) Without $\mathrm{PV}_{\mathrm{linear\ load}}$. (e) With $\mathrm{PV}_{\mathrm{linear\ load}}$. (f) With $\mathrm{PV}_{\mathrm{nonlinear\ load}}$ (Scales: Time: 0.1 s/div., %THD: 0.50%/div.).

TABLE III
SIMULATION THD ANALYSIS

Test cases	Simulation	
	Conventional PI	Proposed
Test case-1 (Change in Irradiance)	3.42%	1.68%
Test case-2 (Dynamic linear load)	3.06%	1.72%
Test case-3 (Dynamic non-linear load)	3.95%	3.75%
Test case-4 (L-G fault)	3.46%	1.57%
Test case-5 (Unbalanced grid voltage)	20.45%	11.45%

TABLE IV
HARDWARE PARAMETERS

Parameter	Value
PV array voltage (V_{pv})	400 V
PV array current (I_{pv})	4 A
DC bus Voltage (V_{dc})	300 V
Grid Inverter Voltage (L-L)	415 V
Grid Inverter Current (L-L)	3 A
Grid Side Inductor (L_f)	20 mH
Grid Side Local Load	0.5 kW (Max)

Test Case 2: In this case, by checking the dynamic performance is investigated by increasing the linear load in the system, which is observed in Fig. 5 during $t = 0.4$–0.8 s. Fig. 5(a) and (b) shows the three-phase currents and voltages under the load change, respectively. The change in the load reflects on the grid currents. Fig. 5(c) and (d) depicts the current and voltage characteristics of the conventional PI controller and the proposed RNN current controller, respectively. By observing Fig. 5(c) and (d), the proposed RNN controller shows better stability performance over the conventional PI controller by maintaining the constant voltage. Similarly, Fig. 5(e) and (f), shows %THD content for the grid current during dynamic load change with PI and proposed RNN controller is 3.06% and 1.72%, respectively. In this condition, THD content of the proposed controller has been found very less compared to the conventional controller.

Test Case 3: In this case, the system dynamic performance is investigated by adding the nonlinear load to the system, which is shown in Fig. 6 during $t = 0.3$–0.8 s. Fig. 6(a) and (b) shows the three-phase grid currents, and voltages under nonlinear load change, respectively. It is evident from the figure that the change in the nonlinear load reflects on the grid currents. Fig. 6(c) and (d) depicts the current and voltage characteristics of the conventional PI controller and proposed RNN current controller, respectively.

By observing Fig. 6(c) and (d), the proposed RNN controller shows better stability and settling performance over the conventional PI controller. Similarly, Fig. 6(e) and (f) shows %THD content for the grid current during transient nonlinear load change with PI and proposed RNN controller is 3.95% and 3.75%, respectively. In this condition, THD content of the proposed controller has been found satisfactorily compared with the conventional controller.

Test Case 4: In this study, an L–G fault is created at grid side during $t = 0.3$–0.8 s. Fig. 7(a) and (b) depicts the three-phase currents and voltages under system fault condition. In this condition, the grid current is raising high because of an L–G fault is created in grid side. Fig. 7(c) and (d) depicts the current and voltage characteristics of the conventional PI controller and

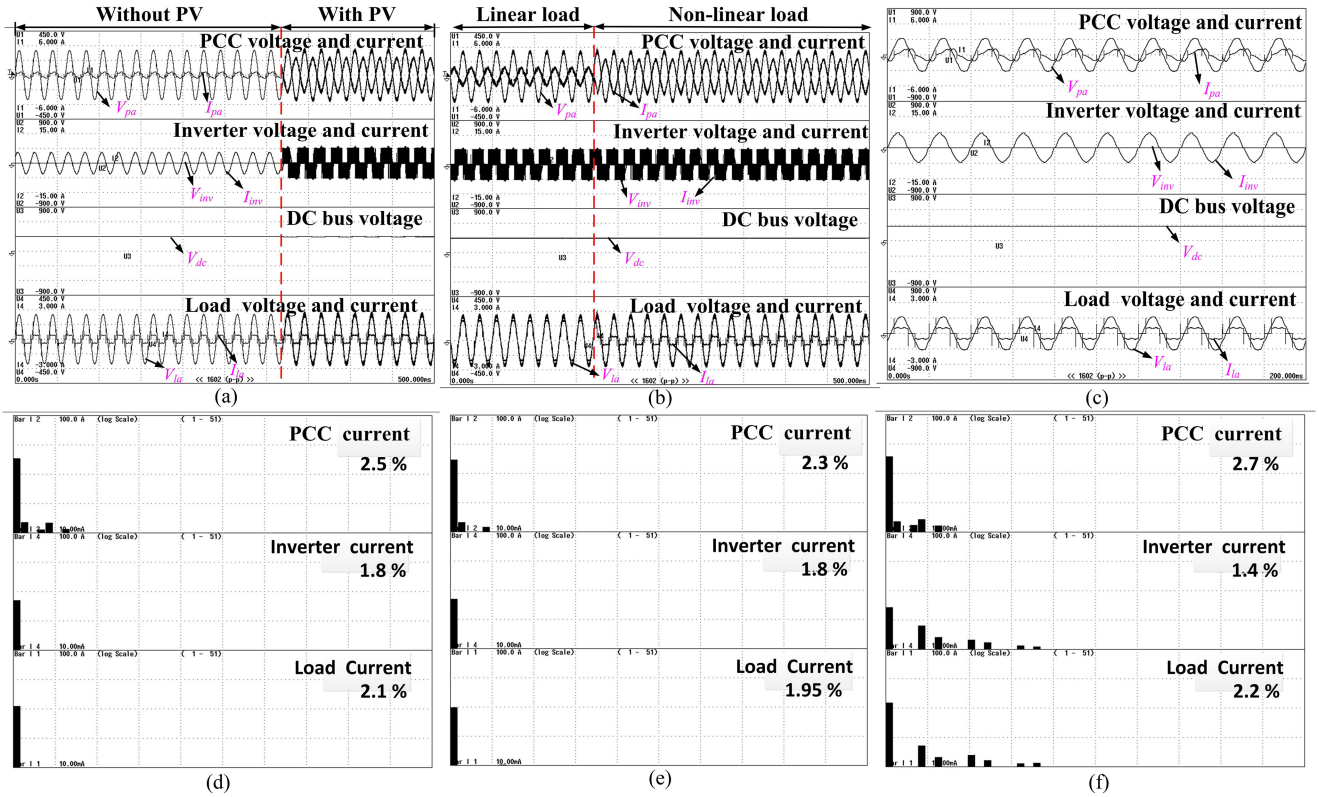

Fig. 12. Performance parameters: (a) PV array integration to grid. (b) Load change from linear to nonlinear. (c) Without $PV_{\text{nonlinear load}}$ (Scales: Time: 0.1 s/div., Voltage: 150 V/div., Current: 1 A/div.). % THD: (d) PV array integration to grid. (e) Load change from linear to nonlinear. (f) Without $PV_{\text{nonlinear load}}$ (Scales: Time: 0.1 s/div., %THD: 1 %/div.).

proposed RNN current controller correspondingly. By observing Fig. 7(c) and (d), the proposed RNN controller shows better performance over the conventional PI controller. Similarly, Fig. 7(e) and (f) shows %THD content for the grid current during an L–G fault condition with PI and proposed RNN controller is 3.46 % and 1.57%, respectively. In this condition, harmonic content of the proposed controller has been found very less compared with the conventional controller.

Test Case 5: In this test case, an unbalanced grid voltage (unequal magnitude and phase) is considered during at $t =$ 0.5–1 s. Fig. 8(a) and (b) shows the three-phase currents and voltages under balanced and unbalanced grid voltage condition, respectively. Fig. 8(c) and (d) depicts the current and voltage characteristics of the conventional PI controller and proposed RNN current controller at the common bus bar. By observing Fig. 8(c) and (d), the conventional PI controller has worse performance under unbalanced voltage condition. However, the proposed RNN controller shows satisfactorily performance over the conventional PI controller. Similarly, Fig. 8(e) and (f) shows %THD content for the grid current during an L–G fault condition with PI and proposed RNN controller is 20.45% and 11.45%, respectively. Finally, it is confirmed that the proposed RNN current controller shows better stability, less damping response, and improved power quality than the conventional PI current controller. Moreover, the stability of the system has maintained well with the proposed controller even under dynamic changes. Also, the high-gain converter has been chosen in this article, which is capable to boost up the PV generated voltage up to 500 V with improved efficiency.

VI. Hardware Analysis

An experimental prototype laboratory setup with PV interfaced system has been developed, which is shown in Figs. 9 and 10, respectively. The main components of the system are as follows, PV panel (1.6 kW), dc–dc boost converter (1.5 kW), inverter module (5 kVA), three-phase load (415 V/10 A), dSPACE Micro lab box (RTI 1202), KEYSIGHT mixed signal oscilloscope (MSOX 2002 A, 70 MHz, 2GSa/s), and YOKOGAWA (WT 1800) precision power analyzer. The proposed RNN-Hebbian-LMS control algorithm has been designed by using the dSPACE interfaced MATLAB/Simulink, and then imported into the dSPACE control desk system as description (.sdf) file. The inputs of the control algorithm are V_{abc}, I_{abc}, and V_{dc}, which are shown in Fig. 9. The input signals are taken as feedback signals from sensor circuit and connected to analog input terminals (IO) of dSPACE kit with BNC cable. The important parameters for the laboratory setup are given in Table III.

The pulses generated by the RNN current controller algorithm are given to the IGBT switches of the inverter through the output ports. Fig. 11(a) shows the voltage and current at PCC, inverter voltage current, dc-bus voltage, and load voltage and current. When PV power is absent, a 600-W load is satisfied by the grid. In the presence of PV array, a linear load of 300 W is satisfied from it, as shown in Fig. 11(b). Similarly, a nonlinear load of 500 W is supplied from PV, as shown in Fig. 11(c). The corresponding %THD for the different currents are shown in Fig. 11(d)–(f).

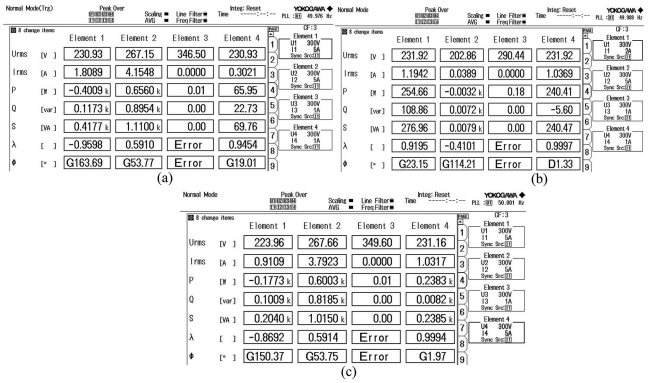

Fig. 13. Powers experimental data.

Fig. 12(a) shows the effect on the system during the integration of PV array. Fig. 12(b) shows the changes occurred in the system during the load change from linear to nonlinear. Also, the effect of nonlinear loads is shown in Fig. 12(c). The respective %THD for the system changes are shown in Fig. 12(d)–(f). Fig. 13 shows the powers experimental data under different conditions. Finally, by observing the results for different system changes, the common bus voltage is maintained constant and the system is stable. The proposed algorithm is able to maintain the stability at different system variations, and the power quality of the system within the limits. Hence, it can be assured that the proposed RNN-Hebbian-LMS is able to integrate to utility grid with improved performance.

VII. Conclusion

Power generation using renewable sources especially solar has been evolving in the present scenario. PV plant integration to the utility grid is limited by few demerits such as low PV terminal voltage and poor power quality under dynamic load changes. To overcome these drawbacks, this work mainly focuses on the performance of using high-gain boost converter with Kalman MPPT to get the high voltage level. In addition, RNN-based current control technique trained with Hebbian-LMS algorithm is used to achieve enhanced power quality, i.e., %THD is well within the limit under various operating scenarios. The simulation and hardware results exhibited the better performance of the proposed controller over conventional one in terms of stability and power quality even under system disturbances. The excellent performance of well-trained RNN current controller using Hebbian-LMS under challenging and distorted operating scenarios indicates the viability of using this controller in real-time applications.

References

[1] S. Manaffam, M. Talebi, A. K. Jain, and A. Behal, "Intelligent pinning based cooperative secondary control of distributed generators for microgrid in islanding operation mode," *IEEE Trans. Power Syst.*, vol. 33, no. 2, pp. 1364–1373, Mar. 2018.

[2] S. Mishra and P. K. Ray, "Power quality improvement using photovoltaic fed DSTATCOM based on JAYA optimization," *IEEE Trans. Sustain. Energy*, vol. 7, no. 4, pp. 1672–1680, Oct. 2016.

[3] R. Langella, A. Testa, J. Meyer, F. Moller, R. Stiegler, and S. Z. Djokic, "Experimental-based evaluation of PV inverter harmonic and interharmonic distortion due to different operating conditions," *IEEE Trans. Instrum. Meas.*, vol. 65, no. 10, pp. 2221–2233, Oct. 2016.

[4] A. Mondal and M. S. Illindala, "Improved frequency regulation in an islanded mixed source microgrid through coordinated operation of DERs and smart loads," *IEEE Trans. Ind. Appl.*, vol. 54, no. 1, pp. 112–120, Jan./Feb. 2018.

[5] P. Siano, "Assessing the impact of incentive regulation for innovation on RES integration," *IEEE Trans. Power Syst.*, vol. 29, no. 5, pp. 2499–2508, Sep. 2014.

[6] S. K. Tiwari, B. Singh, and P. K. Goel, "Design and control of microgrid fed by renewable energy generating sources," *IEEE Trans. Ind. Appl.*, vol. 54, no. 3, pp. 2041–2050, May/Jun. 2018.

[7] H. Du and Z. Huo, "PSM control technique for primary-side regulating fly-back converters," *IET Power Electron.*, vol. 11, no. 3, pp. 531–538, Mar. 20, 2018.

[8] P. N. Babu, B. Kar, and B. Halder, "Comparative analysis of a hybrid active power filter for power quality improvement using different compensation techniques," in *Proc. Int. Conf. Recent Adv. Innovations Eng.*, 2016, pp. 1–6.

[9] M. Das and V. Agarwal, "Design, and analysis of a high-efficiency DC-DC converter with soft switching capability for renewable energy applications requiring high voltage gain," *IEEE Trans. Ind. Electron.*, vol. 63, no. 5, pp. 2936–2944, May 2016.

[10] H. Karmaker, M. Ho, and D. Kulkarni, "Comparison between different design topologies for multi-megawatt direct drive wind generators using improved second generation high temperature superconductors," *IEEE Trans. Appl. Supercond.*, vol. 25, no. 3, pp. 1–5, Jun. 2015, Art. no. 5201605.

[11] P. N. Babu, B. Kar, and B. Halder, "Modelling and analysis of a hybrid active power filter for power quality improvement using hysteresis current control technique," in *Proc. 7th India Int. Conf. Power Electron.*, 2016, pp. 1–6.

[12] W. Wu, Y. Sun, Z. Lin, T. Tang, F. Blaabjerg, and H. S. H. Chung, "A new LCL-filter with in-series parallel resonant circuit for single-phase grid-tied inverter," *IEEE Trans. Ind. Electron.*, vol. 61, no. 9, pp. 4640–4644, Sep. 2014.

[13] Q. Liu, L. Peng, Y. Kang, S. Tang, D. Wu, and Y. Qi, "A novel design, and optimization method of an LCL filter for a shunt active power filter," *IEEE Trans. Ind. Electron.*, vol. 61, no. 8, pp. 4000–4010, Aug. 2014.

[14] A. V. Timbus, R. Teodorescu, F. Blaabjerg, M. Liserre, and P. Rodriguez, "Linear and nonlinear control of distributed power generation systems," in *Proc. IEEE Ind. Appl. Conf. 41st IAS Annu. Meeting*, vol. 2, Dec. 2006, pp. 1015–1023.

[15] N. Mukherjee and D. De, "Analysis, and improvement of performance in LCL filter-based PWM rectifier/inverter application using hybrid damping approach," *IET Power Electron.*, vol. 6, no. 2, pp. 309–325, Feb. 2013.

[16] J. Dannehl, C. Wessels, and F. W. Fuchs, "Limitations of voltage-oriented PI current control of grid-connected PWM rectifiers with LCL filters," *IEEE Trans. Ind. Electron.*, vol. 56, no. 2, pp. 380–388, Feb. 2009.

[17] S. Dasgupta, S. K. Sahoo, and S. K. Panda, "Single-phase inverter control techniques for interfacing renewable energy sources with microgrid—Part I: Parallel-connected inverter topology with active and reactive power flow control along with grid current shaping," *IEEE Trans. Power Electron.*, vol. 26, no. 3, pp. 717–731, Mar. 2011.

[18] E. Corsetti, A. Guagliardi, and C. Sandroni, "Recurrent neural networks for very short term energy resource planning in a microgrid," in *Proc. Mediterranean Conf. Power Gener., Transmiss., Distrib. Energy Convers.*, 2016, pp. 1–9.

[19] M. Liserre, F. Blaabjerg, and S. Hansen, "Design and control of an LCL-filter-based three-phase active rectifier," *IEEE Trans. Ind. Appl.*, vol. 41, no. 5, pp. 1281–1291, Sep./Oct. 2005.

[20] G. Adinolfi, G. Graditi, P. Siano, and A. Piccolo, "Multiobjective optimal design of photovoltaic synchronous boost converters assessing efficiency, reliability, and cost savings," *IEEE Trans. Ind. Informat.*, vol. 11, no. 5, pp. 1038–1048, Oct. 2015.

[21] P. Garanayak and G. Panda, "Fast and accurate measurement of harmonic parameters employing hybrid adaptive linear neural network and filtered-x least mean square algorithm," *IET Gener., Transmiss., Distrib.*, vol. 10, no. 2, pp. 421–436, 2016.

[22] Y. Sun, S. Li, B. Lin, X. Fu, M. Ramezani, and I. Jaithwa, "Artificial neural network for control and grid integration of residential solar photovoltaic systems," *IEEE Trans. Sustain. Energy*, vol. 8, no. 4, pp. 1484–1495, Oct. 2017.

[23] M. E. GamezUrias, E. N. Sanchez, and L. J. Ricalde, "Electrical microgrid optimization via a new recurrent neural network," *IEEE Syst. J.*, vol. 9, no. 3, pp. 945–953, Sep. 2015.

[24] H. R. Baghaee, M. Mirsalim, G. B. Gharehpetian, and H. A. Talebi, "Three-phase AC/DC power-flow for balanced/unbalanced microgrids including wind/solar, droop-controlled and electronically-coupled distributed energy resources using radial basis function neural networks," *IET Power Electron.*, vol. 10, no. 3, pp. 313–328, Oct. 3, 2017.
[25] X. Fu, S. Li, and I. Jaithwa, "Implement optimal vector control for LCL-filter-based grid-connected converters by using recurrent neural networks," *IEEE Trans. Ind. Electron.*, vol. 62, no. 7, pp. 4443–4454, Jul. 2015.
[26] P. N. Babu, P. Rangababu, and G. Panda, "An adaptive differentiation frequency based advanced reference current generator in grid-tied PV applications," *IEEE J. Emerg. Sel. Topics Power Electron.*, to be published, p. 1, Aug. 2019, doi: 10.1109/JESTPE.2019.2933140.
[27] B. O. Kang and J. H. Park, "Kalman filter MPPT method for a solar inverter," in *Proc. IEEE Power Energy Conf. Illinois*, 2011, pp. 1–5.
[28] A. Chaouachi, R. M. Kamel, and K. Nagasaka, "A novel multi-model neuro-fuzzy-based MPPT for three-phase grid-connected photovoltaic system," *Sol. Energy*, vol. 84, no. 12, pp. 2219–2229, 2010.
[29] P. N. Babu, B. C. Babu, P. Rangababu, and G. Panda, "An optimal current control scheme in grid-tied hybrid energy system with active power filter for harmonic mitigation," *Int. Trans. Elect. Energy Syst.*, to be published, 2019, Art. no. e12183, doi: 10.1002/2050-7038.12183.
[30] B. Widrow, Y. Kim, and D. Park, "The Hebbian-LMS learning algorithm," *IEEE Comput. Intell. Mag.*, vol. 10, no. 4, pp. 37–53, Nov. 2015.
[31] S. Jena, G. Panda, and R. Peesapati, "FPGA-based implementation for improved control scheme of grid-connected PV system with 3-phase 3-level NPC-VSI," in *Proc. Int. J. Circthoer Appl.*, 2017, pp. 1–23.
[32] V. Solo, "The stability of LMS," *IEEE Trans. Signal Process.*, vol. 45, no. 12, pp. 3017–3026, Dec. 1997.
[33] I. Nancovska, P. Kranjec, A. Jeglic, and D. Fefer, "Case study of the predictive models used for stability improvement of the DC voltage reference source," *IEEE Trans. Instrum. Meas.*, vol. 47, no. 6, pp. 1487–1491, Dec. 1998.
[34] M. Ghiasi, "Technical and economic evaluation of power quality performance using FACTS devices considering renewable micro-grids," *Renewable Energy Focus*, vol. 29, pp. 49–62, Jun. 2019.
[35] Q. Liu, Y. Li, S. Hu, and L. Luo, "A transformer integrated filtering system for power quality improvement of industrial DC supply system," *IEEE Trans. Ind. Electron.*, to be published, p. 1, May 2019, doi: 10.1109/TIE.2019.2916383.
[36] Q. Liu, Y. Li, L. Luo, Y. Peng, and Y. Cao, "Power quality management of PV power plant with transformer integrated filtering method," *IEEE Trans. Power Del.*, vol. 34, no. 3, pp. 941–949, Jun. 2019.

V. Narendra Kumar received the M.Tech. degree in power and energy systems specialization from the National Institute of Technology Meghalaya, Shillong, India, in 2018.

He is currently a Ph.D. Research Scholar with the Department of Electrical Engineering, Jawaharlal Nehru Technological University Anantapur, Anantapur, India. His current research interests include renewable energy technologies, hybrid ac–dc microgrid, power quality, and control of grid-tied inverters.

Narendra Babu P received the B.Tech. degree in electrical and electronics engineering from Jawaharlal Nehru Technological University, Hyderabad, India, in 2010, and the M.Tech. degree in power and energy systems specialization from the National Institute of Technology Meghalaya, Shillong, India, in 2017.

He is currently a Senior Research Fellow with RECTPCL-CSR Funded Project and the Ph.D. Research Scholar with the Department of Electrical Engineering, National Institute of Technology Meghalaya, Shillong, India. His current research interests include renewable energy technologies, hybrid ac–dc microgrid, power quality, and control of grid-tied inverters.

R. Kiranmayi received the Graduate and M.Tech. degrees in electrical and electronics engineering from Jawaharlal Nehru Technological University, Hyderabad, India, in 1993 and 1995, respectively, and the Ph.D. degree in electrical engineering from Jawaharlal Nehru Technological University, Anantapur, India, in 2013.

She is currently a Professor and the Head of the Department of EEE, College of Engineering, Jawaharlal Nehru Technological University, Anantapur. Her research interests include renewable energy resources and electrical power systems.

Prof. Kiranmayi is a Life Member of ISTE and IEI.

Pierluigi Siano (M'09–SM'14) received the M.Sc. degree in electronic engineering and the Ph.D. degree in information and electrical engineering from the University of Salerno, Salerno, Italy, in 2001 and 2006, respectively.

He is currently a Professor and the Scientific Director of the Smart Grids and Smart Cities Laboratory, Department of Management & Innovation Systems, University of Salerno. He has coauthored more than 450 papers including more than 200 international journal papers that received more than 7200 citations with an H-index equal to 43. His research activities include demand response, integration of distributed energy resources in smart grids, and planning and management of power systems.

Dr. Siano was the recipient of the 2019 highly cited Researcher by ISI Web of Science Group. He has been the Chair of the IES TC on Smart Grids. He is an Editor for the Power & Energy Society Section of IEEE ACCESS, IEEE TRANSACTIONS ON INDUSTRIAL INFORMATICS, IEEE TRANSACTIONS ON INDUSTRIAL ELECTRONICS, OPEN JOURNAL OF THE IEEE IES, and *IET Renewable Power Generation*.

Gayadhar Panda (M'07–SM'19) received the Graduate degree in electrical engineering from the Institute of Engineers, Kolkata, India, in 1996, the master's degree in power electronics from Bengal Engineering College (presently IIEST), Shibpur, India, in 1998, and the Ph.D. degree in electrical engineering from Utkal University, Bhubaneswar, India, in 2007.

He is currently a Professor with the Electrical Engineering Department, National Institute of Technology, Meghalaya, India. He was the Head of the Department, Dean (FW), Chief Vigilance Officer, and the Chairman of various committees at the Institute level. He is currently looking after the responsibility of Dean (AA) at NIT Meghalaya. He has authored/coauthored more than 85 technical papers in national and international conferences proceedings or journals. His work involves design, implementation, and operation of ac/dc microgrid with interfacing converters that use digital signal processing, artificial intelligence techniques, and other novel control methods. His research interests include the areas of automatic generation control, stability improvements using FACT devices, power quality control, distributed power generation, and power electronics and drives.

Dr. Panda is a recipient of the institution medal for his outstanding research work at NIT Meghalaya. He has won the Power Medal for his one of the research paper from IE (India). He has more than 20 years of teaching experience.